

Cite this: *Dalton Trans.*, 2021, **50**,
3682

Selectivity-tunable oxidation of tetrahydro- β -carboline over an OMS-2 composite catalyst: preparation and catalytic performance†

Xiuru Bi,^{a,b} Luyao Tao,^{a,b} Nan Yao,^a Mingxia Gou,^a Gexin Chen,^a Xu Meng ^{*a} and Peiqing Zhao^{*a}

Controlling the reaction selectivity of organic transformations without losing high conversion is always a challenge in catalytic processes. In this work, a $\text{H}_3\text{PO}_4\cdot 12\text{WO}_3/\text{OMS-2}$ nanocomposite catalyst ([PW]-OMS-2) was prepared through the oxidation of a Mn(II) salt with sodium phosphotungstate by KMnO_4 . Comprehensive characterization indicates that different Mn^{2+} precursors significantly affected the crystalline phase and morphology of the as-synthesized catalysts and only $\text{MnSO}_4\cdot\text{H}_2\text{O}$ as the precursor could lead to a cryptomelane phase. Moreover, [PW]-OMS-2 demonstrated excellent catalytic activity toward aerobic oxidative dehydrogenation of tetrahydro- β -carbolines due to mixed crystalline phases, enhanced surface areas, rich surface oxygen vacancies and labile lattice oxygen species. In particular, β -carbolines and 3,4-dihydro- β -carbolines could be obtained from tetrahydro- β -carbolines with very high selectivity (up to 99%) over [PW]-OMS-2 *via* tuning the reaction solvent and temperature. Under the present catalytic system, scalable synthesis of a β -carboline was achieved and the composite catalyst showed good stability and recyclability. This work not only clarified the structure–activity relationship of the catalyst, but also provided a practical pathway to achieve flexible, controllable synthesis of functional N-heterocycles.

Received 18th January 2021,
Accepted 12th February 2021

DOI: 10.1039/d1dt00168j

rsc.li/dalton

Introduction

The β -carboline skeleton is one of the most intriguing indole alkaloids which are widely present in marine organisms, plants, microorganisms, and fungi.^{1,2} In particular, aromatic β -carboline compounds have attracted much attention due to their excellent biological and pharmaceutical activities, such as antimalarial,³ antibacterial,⁴ antitumor,⁵ and anti-HIV activities.^{3,6} Besides, some β -carboline derivatives can be used as potential therapeutic agents for neurodegenerative disorders, such as Alzheimer's and Parkinson's disease,⁷ because of the inhibition of acetylcholinesterase⁸ and human monoamine oxidase.⁹ Besides β -carbolines, 3,4-dihydro- β -carbolines can be used as exclusive intermediates for the synthesis of pharmaceutical molecules *via* further modification.¹⁰ In view of the important pharmacological properties of β -carbolines, many synthetic methods have been developed so far.^{11–20} One classical approach to generate tetrahydro- β -carbolines is

Pictet–Spengler reaction between a tryptamine derivative and an aldehyde or carboxylic acid followed by oxidative dehydrogenation to provide the corresponding β -carbolines and 3,4-dihydro- β -carbolines.^{21–23} According to the report, the traditional process of aerobic oxidative dehydrogenation is usually carried out by heating with palladium on carbon²⁴ or toxic sulfur,^{5,22} or treating with strong stoichiometric oxidants such as SeO_2 ,²⁵ MnO_2 ,²⁶ and KMnO_4 ²⁰ at high temperature over a prolonged time. Besides, dichlorodicyanoquinone (DDQ),²⁷ trichloroisocyanuric acid (TCCA),²⁸ (diacetoxyiodo)benzene $\text{PhI}(\text{OAc})_2$,²¹ *N*-chlorosuccinimide (NCS),^{29,30} and 2-iodoxybenzoic acid (IBX)³¹ have also been used to perform oxidative dehydrogenation, but these methods suffer from drawbacks such as the use of excess reagents, generation of stoichiometric waste, poor yields and a lack of practicability. In particular, there are no reports on selectivity-tunable oxidative synthesis of β -carbolines and 3,4-dihydro- β -carbolines to date. Therefore, it is of great practical significance to develop an efficient, high chemoselectivity, and environmentally friendly method for syntheses of β -carbolines and 3,4-dihydro- β -carbolines.

Manganese oxide octahedral molecular sieve (OMS-2) is a cryptomelane-type microporous nanostructural manganese oxide, which is formed of 2×2 edge-shared MnO_6 octahedral chains and composed of corner-connected MnO_6 octahedral to

^aState Key Laboratory for Oxo Synthesis and Selective Oxidation, Suzhou Research Institute of LICP, Lanzhou Institute of Chemical Physics (LICP), Chinese Academy of Sciences, Lanzhou 730000, China. E-mail: xumeng@licp.cas.cn, zhaopq@licp.cas.cn

^bUniversity of Chinese Academy of Sciences, Beijing 100049, China

† Electronic supplementary information (ESI) available: Experimental procedures and data. See DOI: 10.1039/d1dt00168j

form $4.6 \times 4.6 \text{ \AA}$ tunnels.^{32–35} Manganese is present in OMS-2 as Mn^{2+} , Mn^{3+} , and Mn^{4+} , and K^+ exists in the tunnels to balance the whole valence state and stabilize the tunnel structure.^{36–39} Due to its unique structural properties, redox ability, adsorption, ion-exchange, and semiconductivity, OMS-2 has been widely applied to environmental catalysis, electrode materials, semiconductors, separation, organic synthesis and many other fields.^{40–46} Because of abundant oxygen vacancy and mixed-valence Mn ions on the surface, OMS-2 is able to readily activate O_2 or H_2O_2 used as a green oxidant in clean synthesis of organic molecules.⁴⁷ In the past years, our group has focused on the fabrication and modification of materials involving OMS-2 and their catalytic application in the clean synthesis of heterocycles.^{48–51} To effectively improve the selectivity and conversion of organic synthesis, the development of new catalysts, modification of pathways and tuning catalytic systems are meaningful.

Very recently, we have prepared an OMS-2-based nanocomposite doped with sodium phosphowolframate for the first time and applied it to the aerobic oxidative dehydrogenation of N-heterocycles.⁴⁸ Sufficient characterization indicated that the catalyst had newly generated mixed crystal phases of $\text{H}_3\text{PO}_4 \cdot 12\text{WO}_3$ and cryptomelane by doping of 2 mol% sodium phosphowolframate, which was critical for the superior catalytic performance. Kinetic studies showed that the presence of the mixed crystal could significantly increase the initial reaction rate and decrease the apparent activation energy of oxidation reaction. To develop a new synthetic strategy for 3,4-dihydro- β -carboline and β -carboline compounds, we attempted to selectively oxidize tetrahydro- β -carbolines over OMS-2 doped with sodium phosphotungstate.

OMS-2 materials are usually prepared *via* the oxidation reaction between Mn^{2+} and KMnO_4 . Different Mn^{2+} precursors can have various effects on the physicochemical properties of the catalyst, for example, the crystal phase, surface area, and redox properties, and consequently affect the catalytic performance.⁵² In this work, we investigated the effects of Mn^{2+} precursors on the preparation of OMS-2 doped with 2 mol% sodium phosphotungstate to obtain the optimal hybrid catalyst with a synergistic effect of mixed phases. With the as-synthesized OMS-2 nanocomposite, selectivity-tunable oxidative dehydrogenation of tetrahydro- β -carbolines was realized for the first time through tuning the catalytic system.

Experimental

General information

All chemicals used here were of analytical grade, were purchased from commercial suppliers and were used without further purification. All experiments were carried out under air or under an O_2 balloon. Standard column chromatography was performed on 200–300 mesh silica gel (obtained from Merck) using flash column chromatography techniques. ^1H and ^{13}C NMR spectra for compound characterization were recorded on WNMN-1 500. Chemical shift values are given in parts per

million relative to the residual solvent peaks CDCl_3 and $(\text{CD}_3)_2\text{SO}$. Chemical shifts of ^1H NMR spectra were recorded relative to TMS (δ 0.00) or residual deuterated solvents (CDCl_3 : δ 7.26; $(\text{CD}_3)_2\text{SO}$: δ 2.50). Chemical shifts of ^{13}C NMR spectra were recorded relative to solvent resonance (CDCl_3 : δ 77.16; $(\text{CD}_3)_2\text{SO}$: δ 39.52).

Catalyst preparation

All the OMS-2-based composites (2 mol% of dopant to the amount of KMnO_4) in the present research were prepared *via* the reaction between Mn^{2+} and potassium permanganate with a reflux method. Taking $\text{MnSO}_4 \cdot \text{H}_2\text{O}$ as a Mn^{2+} precursor, the typical procedure was as follows: in a round bottom flask, $\text{MnSO}_4 \cdot \text{H}_2\text{O}$ (8.80 g, 52 mmol) and sodium phosphotungstate (2.18 g, 0.74 mmol) were dissolved in 30 mL of deionized water followed by the addition of 3 mL of HNO_3 at room temperature. Then, 100 mL of KMnO_4 (5.89 g, 37 mmol) solution was added dropwise into the above solution under vigorous stirring at room temperature. After the resulting solution was refluxed at 100 °C for 24 h, the resulting solid was collected by filtration, washed with deionized water, dried in air at 80 °C for 8 h, and ground into a powder to afford the OMS-2-based nanocomposite which was labeled as [PW]-OMS-2. When MnCl_2 , $\text{Mn}(\text{NO}_3)_2$, $\text{Mn}(\text{Ac})_2$, MnCO_3 , and anhydrous MnSO_4 were used as precursors, the catalytic materials prepared were labeled as [PW]-OMS-2-Cl, [PW]-OMS-2-NO, [PW]-OMS-2-Ac, [PW]-OMS-2-CO, and [PW]-OMS-2-SO, respectively.

General procedure for [PW]-OMS-2-catalyzed 3,4-dihydro- β -carboline synthesis

Typically, a mixture of [PW]-OMS-2 (20 mg, 13 mol%), tetrahydro- β -carbolines (0.2 mmol), and 1 mL mixture solvent of acetonitrile/toluene ($v/v = 1/1$) in a reaction tube was magnetically stirred at 80 °C for 8 h in air. The reaction process was monitored by thin layer chromatography (TLC). After completion of the reaction, the reaction mixture was diluted with ethyl acetate and filtered. The filtrate was removed using a rotary evaporator at reduced pressure, and then the pure product was obtained by silica gel column chromatography (petroleum/ethyl acetate = 5/1 as the eluent). The composition and structure of target products were determined by ^1H and ^{13}C NMR spectroscopy.

General procedure for [PW]-OMS-2-catalyzed β -carboline synthesis

[PW]-OMS-2 (20 mg, 13 mol%), tetrahydro- β -carboline compounds (0.2 mmol), and 1.0 mL *o*-dichlorobenzene were added into a reaction tube. The mixture was stirred at 130 °C under air for the indicated time. After completion of the reaction, the reaction mixture was cooled to ambient temperature. Then, the reaction mixture was diluted with ethyl acetate and filtered. The resulting filtrate was concentrated under reduced pressure to give the crude product which was purified by silica gel chromatography to yield the pure product.

Catalyst characterization

The XRD patterns of the as-prepared catalysts were collected using powder X-ray diffraction with an X-Pert PRO X-ray diffractometer using Cu K α radiation ($\lambda = 0.15406$ nm). The data of 2θ from 5 to 80° were collected with a step size of 0.065°. X-ray photoelectron spectroscopy (XPS) analysis was conducted on a Kratos AXIS Ultra DLD high-performance electron spectrometer operated at a pass energy of 30 eV with Al K α ($\lambda = 1486.7$ eV) as an exciting X-ray source. The binding energy was calibrated with the contaminant carbon value of 284.8 eV. The specific surface areas of the catalysts were determined from N₂ adsorption/desorption analysis at 76 K using an ASAP 2020 M analyzer. The samples were first pretreated at 300 °C for 4 hours before measurements. The specific surface areas were determined utilizing the BET model for the calculation of specific surface areas. The morphology was observed with FE-SEM (Quanta 400FEG) and HRTEM (Tecnai G2 F20 S-Twin 200 kV).

Results and discussion

Characterization of [PW]-OMS-2 composite catalysts

OMS-2 composite catalysts ([PW]-OMS-2) were synthesized and obtained by the use of different Mn(II) salts, including MnCl₂, Mn(NO₃)₂, Mn(Ac)₂, MnCO₃, MnSO₄·H₂O and anhydrous MnSO₄, with sodium phosphotungstate as the dopant. XRD patterns of the as-prepared catalysts derived from different Mn²⁺ precursors are depicted in Fig. 1. From the analysis of XRD spectra, it was found that the catalysts prepared from MnSO₄ or MnSO₄·H₂O were well crystallized with the cryptomelane structure, characteristic of the octahedral molecular sieve material (JCPDS file #29-1020). In addition, [PW]-OMS-2 also showed the mixed crystal phase of phosphotungstic acid (H₃O₄₀PW₁₂·xH₂O, JCPDS file #38-178). When anhydrous MnSO₄ was used as the precursor, the crystal type of phosphotungstic acid was more obvious. However, the diffraction peaks of [PW]-OMS-2-Cl, [PW]-OMS-2-NO, [PW]-OMS-2-Ac, and [PW]-

OMS-2-CO had the same ϵ -MnO₂ phase (JCPDS file #30-820). The sizes of the as-prepared catalyst materials with different precursors were calculated from the line broadening of XRD peaks using Scherrer's formula ($d = 0.9\lambda/\beta \cos \theta$). The as-calculated crystal sizes of [PW]-OMS-2-Cl, [PW]-OMS-2-NO, [PW]-OMS-2-Ac, [PW]-OMS-2-CO, [PW]-OMS-2-SO, and [PW]-OMS-2 were 13.5, 10.2, 12.1, 11.7, 10.3, and 9.1 nm, respectively. These observations suggested that Mn²⁺ precursors directly affected the crystalline structure. Among the tested Mn(II) salts, just manganese sulfate (with or without crystal water) was able to afford cryptomelane-type OMS-2.

Subsequently, the BET surface areas and porosities of the [PW]-OMS-2 materials were determined by N₂ adsorption-desorption, and the results are presented in Table 1. Compared with original OMS-2, it is obvious to summarize that the dopant of sodium phosphotungstate significantly enhanced the BET surface area. The influence of surface area on the catalytic materials prepared with different Mn²⁺ precursors was different. Among them, the as-synthesized materials with the ϵ -MnO₂ crystal phase had similar specific surface areas (188–224 m² g⁻¹). Although [PW]-OMS-2-SO and [PW]-OMS-2 had similar mixed crystal phases of cryptomelane and phosphotungstic acid, the latter (204 m² g⁻¹) was twice as large as the former (102 m² g⁻¹). The remarkable difference in surface areas between [PW]-OMS-2-SO and [PW]-OMS-2 further indicated the notable effect of Mn²⁺ precursors for the synthesis of the catalyst. Mn²⁺ precursors not only influenced the crystal structure of the products, but also altered their textural properties. Generally, the catalytic performance of catalytic materials is closely related to their surface areas, and a higher surface area tends to expose more catalytically active sites to enhance the catalytic performance.

In our previous study, the oxygen and metal species on the surface of the catalyst have a vital influence on the catalytic performance in oxidation reactions.^{47–51} Therefore, X-ray photoelectron spectroscopy was employed to analyze the surface elemental species (Fig. 2 and 3, Tables 1 and 2). [PW]-OMS-2-Cl, [PW]-OMS-2-NO, [PW]-OMS-2-Ac and [PW]-OMS-2-CO with ϵ -MnO₂ phases all showed similar contents of different valences of manganese. Due to the influence of

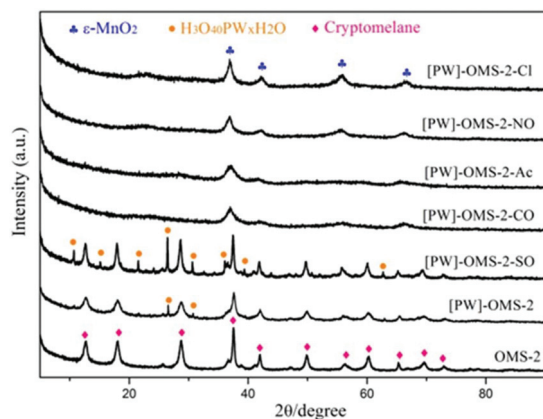


Fig. 1 XRD patterns of the [PW]-OMS-2 catalysts synthesized using different Mn²⁺ precursors.

Table 1 Textural properties of OMS-2 and the [PW]-OMS-2 catalysts

Catalyst	Surface area (m ² g ⁻¹)	Pore volume (cm ³ g ⁻¹)	Pore size (nm)	AOS ^a
OMS-2	67	0.37	28	3.83 ^b
[PW]-OMS-2-Cl	188	0.51	11	3.39
[PW]-OMS-2-NO	193	0.56	12	3.36
[PW]-OMS-2-Ac	207	0.39	8	3.28
[PW]-OMS-2-CO	224	0.35	6	3.40
[PW]-OMS-2-SO	102	0.34	13	3.39
[PW]-OMS-2	204	0.59	13	3.65

^a Average oxidation state (AOS) of Mn was calculated according to the binding energy difference (ΔE) of Mn 3s in XPS through an empirical formula, *i.e.* AOS = 8.956–1.126 × ΔE . ΔE : the splitting width (Δ) of the XPS spectra in the Mn 3s region. ^b AOS determination by the magnetic method.⁵³

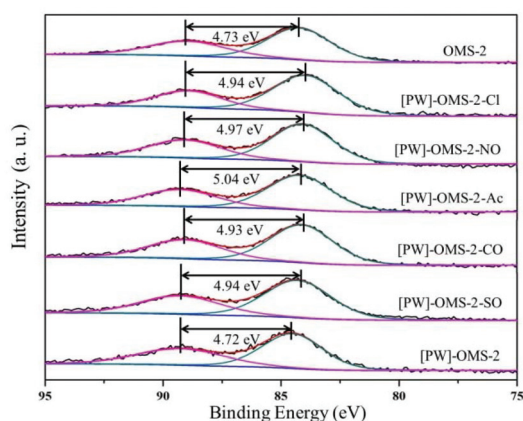


Fig. 2 The Mn 3s XPS patterns of the as-synthesized materials.

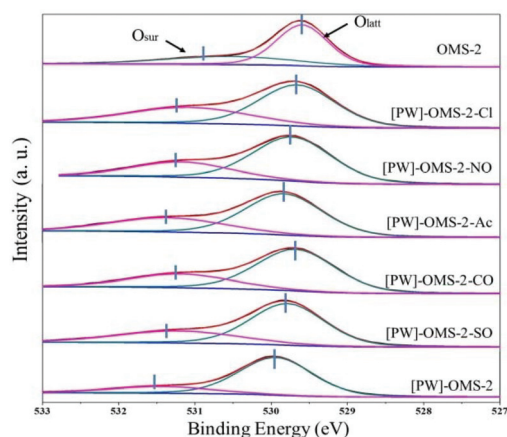


Fig. 3 The O 1s XPS patterns of the as-synthesized materials.

complex multiplet splitting, binding energy values overlapping and the loss of the satellite peak, it is hard to calculate the valence of manganese from Mn 2p. Instead, the average oxidation state (AOS) can more accurately reflect the oxidation state of the Mn species.⁵⁴ Through the analysis of the Mn 3s XPS spectra, the average oxidation state (AOS) of Mn was calculated based on the following formula: $AOS = 8.956 - 1.126 \times \Delta E$, where ΔE is the binding energy difference between the doublet Mn 3s peaks as shown in Fig. 2. Compared with the original OMS-2, the AOS of [PW]-OMS-2 materials decreased to different degrees, while only [PW]-OMS-2 showed a slight decrease. Next, the O 1s XPS spectra were fitted into two peaks including surface adsorbed unsaturated oxygen species with high binding energy and saturated lattice oxygen with low binding energy (Fig. 3 and Table 2). We can see an obvious shift of the lattice oxygen peak on comparing [PW]-OMS-2 with the other OMS-2-based materials and original OMS-2, which means that there are weaker interactions between Mn and O atoms and the reactivity of lattice oxygen improved. Moreover, [PW]-OMS-2 showed the highest content of lattice oxygen species (80.4%) compared with others.

Table 2 The O 1s XPS of the as-synthesized materials

Catalyst	Binding energy of O 1s (eV)		Oxygen species (%)	
	Surface O	Lattice O	Surface O	Lattice O
OMS-2	531.12	530.03	33.6	66.4
[PW]-OMS-2-Cl	531.08	529.66	38.1	61.9
[PW]-OMS-2-NO	531.17	529.72	29.6	70.4
[PW]-OMS-2-Ac	531.36	529.83	33.5	66.5
[PW]-OMS-2-CO	531.18	529.68	29.8	70.2
[PW]-OMS-2-SO	531.21	529.79	32.2	67.8
[PW]-OMS-2	531.43	529.94	19.6	80.4

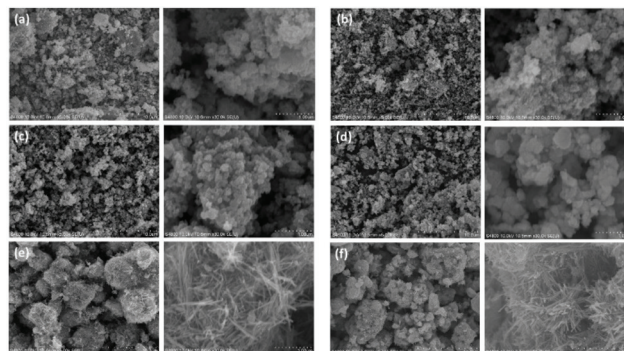


Fig. 4 SEM images of (a) [PW]-OMS-2-Cl, (b) [PW]-OMS-2-NO, (c) [PW]-OMS-2-Ac, (d) [PW]-OMS-2-CO, (e) [PW]-OMS-2-SO, and (f) [PW]-OMS-2.

The effect of different Mn^{2+} precursors on MnO_2 crystal growth was also observed with SEM (Fig. 4) and TEM (Fig. 5). SEM diagrams showed that [PW]-OMS-2-Cl, [PW]-OMS-2-NO, [PW]-OMS-2-Ac, and [PW]-OMS-2-CO were composed of nanoparticles and some clusters. However, both [PW]-OMS-2-SO and [PW]-OMS-2 showed a typical uniform nanorod mor-

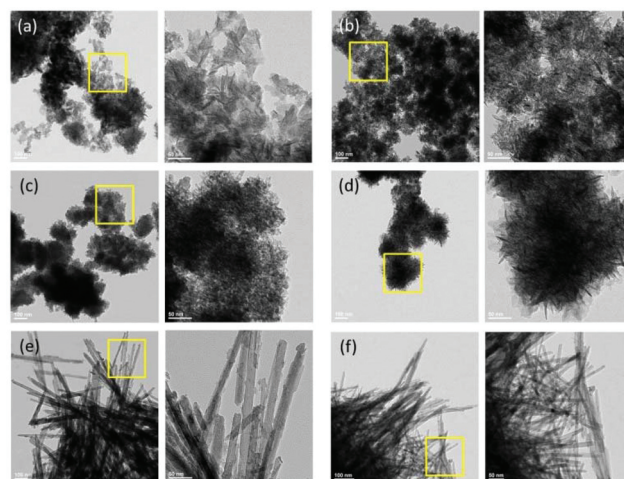


Fig. 5 TEM images of (a) [PW]-OMS-2-Cl, (b) [PW]-OMS-2-NO, (c) [PW]-OMS-2-Ac, (d) [PW]-OMS-2-CO, (e) [PW]-OMS-2-SO, and (f) [PW]-OMS-2.

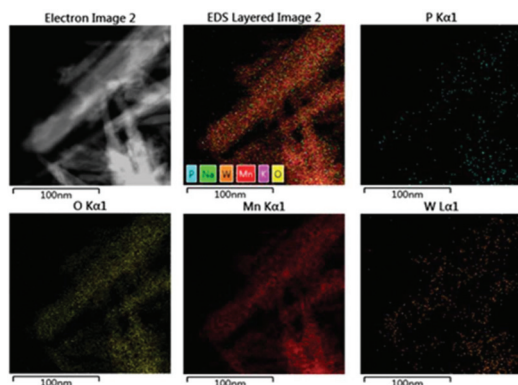


Fig. 6 Element mapping of [PW]-OMS-2.

phology that was the same as original OMS-2 (Fig. S1 in the ESI†). These results on morphology mean that with anhydrous MnSO_4 or $\text{MnSO}_4 \cdot \text{H}_2\text{O}$ as the Mn^{2+} precursor, sodium phosphotungstate doping did not change the structure and morphology of OMS-2-based composites. From the TEM images (Fig. 4), it was found that [PW]-OMS-2-Cl, [PW]-OMS-2-NO, [PW]-OMS-2-Ac, and [PW]-OMS-2-CO all had lamellar structures that were the same as that of a typical ϵ - MnO_2 material.^{55,56} For [PW]-OMS-2-SO, an irregular surface of OMS-2 nanorods could be observed, which might be phosphotungstic acid generated *in situ* from sodium phosphotungstate coordinated with MnO_6 uniting on the nanorods (Fig. 5e). However, [PW]-OMS-2 had a relatively smooth surface as observed from the TEM images (Fig. 5f). These observations were in accordance with the XRD patterns of [PW]-OMS-2-SO and [PW]-OMS-2, and the former had much stronger diffraction peaks of phosphotungstic acid than the latter (Fig. 1).

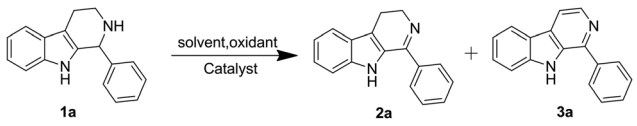
Lastly, [PW]-OMS-2 was selected as a sample for EDX analysis because it had the mixed crystal phases with the largest surface area and the most potential catalytic ability based on XPS analysis (Fig. 6). EDX results illustrated that the doped elements (P and W) were evenly distributed on the catalyst surface. However, no Na ions existed on the sample (Table S1 in the ESI†). Taking the aforementioned characterization into account, phosphotungstic acid formed *in situ* from the decomposition of sodium phosphotungstate coordinated with OMS-2 nanorods to generate the $\text{H}_3\text{PO}_4 \cdot 12\text{WO}_3/\text{OMS-2}$ nanocomposite material.

Catalytic activity of [PW]-OMS-2 composite materials

In order to examine the activity of the as-synthesized catalysts using different precursors for selective oxidative dehydrogenation of tetrahydro- β -carbolines, we initially tested different [PW]-OMS-2 materials with 1-phenyl-tetrahydro- β -carboline as the substrate. Firstly, a blank experiment was performed to test whether the substrate was converted without any catalyst. The reaction tube containing 1 mL *o*-dichlorobenzene as the reaction solvent and 0.2 mmol substrates was stirred at 130 °C for 8 h, and there was no substrate conversion (Table 3, entry

1). When the raw material and the dopant of the catalyst, such as $\text{H}_3\text{PO}_4 \cdot 12\text{WO}_3$, KMnO_4 and $\text{MnSO}_4 \cdot \text{H}_2\text{O}$, were added respectively to the reaction system as the catalyst, unsatisfactory conversions and selectivities of **2a** and **3a** were observed (Table 3, entries 2–4). The catalytic effectiveness of the OMS-2 and $\text{H}_3\text{PO}_4 \cdot 12\text{WO}_3$ mixture is similar to that of single OMS-2. That is possibly because simple physical mixing did not change the structure and enhance the performance of OMS-2 (Table 3, entries 5 and 6). Subsequently, the original OMS-2 and [PW]-OMS-2 catalytic materials prepared from different precursors were used in the catalytic system to test their activity (Table 3, entries 7–12). Among them, the reaction catalyzed by OMS-2 achieved 72% conversion, 57% selectivity of **2a**, and 43% selectivity of **3a**. For the catalytic material prepared with MnCO_3 as the precursor, the substrate conversion was 79%, and the main product was 3,4-dihydro- β -carboline **2a** (Table 3, entry 9). In the presence of [PW]-OMS-2-Ac, no dehydrogenation products were obtained in spite of high conversion of the substrate (Table 3, entry 10). The rest of the catalysts using different Mn^{2+} precursors all showed moderate or good substrate conversion, and the main dehydrogenation product was β -carboline **3a** (Table 3, entries 7, 8 and 11). In particular, [PW]-OMS-2 facilitated the reaction with the highest catalytic activity and **3a** was obtained at $\sim 100\%$ conversion with 99% selectivity (Table 3, entry 12). These experimental results indicated that only cryptomelane-type OMS-2 catalysts with mixed crystal phases could give 100% conversion of **1a** with excellent selectivity of **3a** compared with ϵ - MnO_2 type catalysts. Meanwhile, we can conclude that more abundant oxygen vacancy on the catalyst, like [PW]-OMS-2, led to high conversion in the oxidation (Table 3, entry 6 *vs.* entry 12). Moreover, appropriate mixed crystal phases of OMS-2 and phosphotungstic acid and surface area could influence the selectivity of the reaction (Table 3, entry 11 *vs.* entry 12).

So far, we determined that [PW]-OMS-2 was the optimal catalyst. Then, we further optimized the reaction conditions. We tried to use oxygen, hydrogen peroxide and air as oxidants, respectively, and the results showed that the oxidative dehydrogenation reaction had the highest conversion and selectivity in air (Table 3, entries 12–14). The results showed that the reaction was much worse in N_2 compared with that in air, which means that the reaction was aerobic oxidation (Table 3, entry 15). Next, a lot of polar solvents were examined to further improve the yield of **3a** at 130 °C with [PW]-OMS-2 (Table 3, entries 16–18). It was found that *o*-dichlorobenzene gave the highest conversion of **1a** ($\sim 100\%$) and selectivity of **3a** (99%) within 8 h (Table 3, entry 12). Under the same reaction conditions, we decreased the reaction temperature to 80 °C, and the results showed that the conversion of **1a** was reduced to 85% and the selectivity of **3a** was 66% (Table 3, entry 19). When using some solvents with relatively low boiling points in the catalytic system, the selectivity of the reaction was changed and the main product was 3,4-dihydro- β -carboline **2a** rather than **3a**. Acetonitrile gave the highest selectivity of **2a** (82%) but 58% conversion of **1a**, while toluene gave the highest conversion of **1a** ($\sim 100\%$) but medium selectivity of **2a** (68%)

Table 3 Optimization of the reaction conditions^a


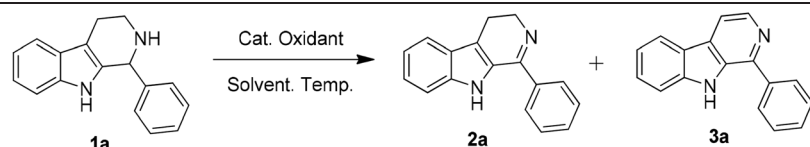
Entry	Catalyst	Temp. (°C)	Solvent	Oxidant	Con. (%)	Sel. of 2a (%)	Sel. of 3a (%)
1	—	130	<i>o</i> -Dichlorobenzene	Air	N.R.	—	—
2 ^b	H ₃ PO ₄ ·12WO ₃	130	<i>o</i> -Dichlorobenzene	Air	26	32	68
3 ^c	KMnO ₄	130	<i>o</i> -Dichlorobenzene	Air	42	29	71
4 ^d	MnSO ₄ ·H ₂ O	130	<i>o</i> -Dichlorobenzene	Air	N.R.	—	—
5	OMS-2	130	<i>o</i> -Dichlorobenzene	Air	72	57	43
6	H ₃ PO ₄ ·12WO ₃ /OMS-2	130	<i>o</i> -Dichlorobenzene	Air	69	54	46
7	[PW]-OMS-2-Cl	130	<i>o</i> -Dichlorobenzene	Air	97	11	89
8	[PW]-OMS-2-NO	130	<i>o</i> -Dichlorobenzene	Air	~100	6	94
9	[PW]-OMS-2-CO	130	<i>o</i> -Dichlorobenzene	Air	79	95	5
10	[PW]-OMS-2-Ac	130	<i>o</i> -Dichlorobenzene	Air	~100	—	—
11	[PW]-OMS-2-SO	130	<i>o</i> -Dichlorobenzene	Air	~100	12	88
12	[PW]-OMS-2	130	<i>o</i> -Dichlorobenzene	Air	~100	—	>99
13 ^e	[PW]-OMS-2	130	<i>o</i> -Dichlorobenzene	O ₂	82	24	76
14 ^f	[PW]-OMS-2	130	<i>o</i> -Dichlorobenzene	H ₂ O ₂	~100	49	51
15 ^g	[PW]-OMS-2	130	<i>o</i> -Dichlorobenzene	N ₂	35	47	53
16	[PW]-OMS-2	130	DMF	Air	~100	55	45
17	[PW]-OMS-2	130	DMSO	Air	~100	18	82
18	[PW]-OMS-2	130	Chlorobenzene	Air	83	78	22
19	[PW]-OMS-2	80	<i>o</i> -Dichlorobenzene	Air	85	34	66
20	[PW]-OMS-2	80	DMC	Air	87	79	21
21	[PW]-OMS-2	80	1,4-Dioxane	Air	89	73	27
22	[PW]-OMS-2	80	Acetonitrile	Air	58	82	18
23	[PW]-OMS-2	80	Toluene	Air	~100	68	32
24 ^h	[PW]-OMS-2	80	Acetonitrile: methylbenzene	Air	95	99	—

^a Reaction conditions: substrate (0.2 mmol), [PW]-OMS-2 (20 mg, 13 mol%), solvent 1 mL, air (1 atm), 80 °C, 8 h. “—” means there is no corresponding product obtained. ^b H₃PO₄·12WO₃ (1.5 mg, 2.6 mol%). ^c KMnO₄ (4.1 mg, 13 mol%). ^d MnSO₄·H₂O (4.4 mg, 13 mol%). ^e O₂ balloon. ^f H₂O₂ (50 μL). ^g N₂ balloon. ^h Methylbenzene: acetonitrile = 0.5 mL: 0.5 mL.

(Table 3, entries 20–24). Therefore, the mixed solvent of acetonitrile and toluene probably could efficiently transform 1a and give 2a in high yield, because toluene was suitable for the conversion of 1a while acetonitrile was superior for the partial oxidative dehydrogenation. As expected, when we added 0.5 mL

acetonitrile into 0.5 mL toluene as a mixed solvent in the reaction, the desired dehydrogenation product 2a was obtained with 99% selectivity with a 95% conversion of 1a (Table 3, entry 24). As a result of the optimization, the two best reaction conditions were as follows: (a) the use of [PW]-OMS-2 as the

Table 4 Conversion and selectivity comparison of this work with those of other reported catalytic systems



Reaction conditions	Reaction temperature (°C)	Reaction time (h)	Yield of 2a (%)	Yield of 3a (%)	Ref.
[PW]-OMS-2(13 mol%)	130	8	— ^a	>99	This work
[PW]-OMS-2(13 mol%)	80	8	94	—	This work
I ₂ (50 mol%), H ₂ O ₂ (1.0 eq.) ²³	100	8	90	—	23
Trichloroisocyanuric acid (0.7 eq.) ¹⁰	25	2	—	88	10
2-Iodoxybenzoic acid (2.5 eq.), TBAB (0.5 eq.) ³¹	25	13	—	60	31
Dess–Martin periodinane (5.5 eq.) ³¹	25	24	—	70	31
Ag ₂ CO ₃ (2.0 eq.), Li ₂ CO ₃ (2.0 eq.) ¹³	160	16	—	70	13
I ₂ (1.5 eq.), TFA (1.0 eq.) ⁵⁷	120	24	—	52	56
CuBr ₂ (20 mol%), DBU (2.0 eq.) ⁵⁸	25	18	—	95	57
N-Chlorosuccinimide (2.1 eq.), TEA (2.5 eq.) ⁵⁹	25	0.5	—	85	58

^a “—” means there is no corresponding product obtained.

catalyst at 130 °C in *o*-dichlorobenzene for obtaining complete dehydrogenation product β -carboline **3a** (Table 1, entry 12); and (b) the use of [PW]-OMS-2 as the catalyst at 80 °C in a mixed solvent of acetonitrile/toluene (v/v = 1/1) for obtaining partial dehydrogenation product 3,4-dihydro- β -carboline **2a**

(Table 1, entry 24). Then, we compared our catalytic selectivity with the previous reports on oxidative dehydrogenation of 1-aryl-tetrahydro- β -carboline (Table 4). To date, there is no report that can realize a selectivity-tunable reaction process for dehydrogenation of tetrahydro- β -carbolines. The comparison

Table 5 Scope of oxidative dehydrogenation to obtain 3,4-dihydro-1-aryl- β -carbolines^a

Entry	Substrate	Product	Con. (%)	Sel. (%)	TON ^b
1			95	99	7.0
2			91	89	6.7
3			96	99	7.1
4			86	99	6.3
5			84	79	6.2
6			81	94	6.0
7			>99	>99	7.2
8			88	98	6.5
9			93	84	6.8
10			95	89	7.0
11			78	92	5.7

^a Reaction conditions: substrate (0.2 mmol), [PW]-OMS-2 (20 mg), toluene: acetonitrile = 0.5 mL: 0.5 mL, air (1 atm), 80 °C, 8 h. ^b Turn over number, TON = moles of tetrahydro- β -carbolines converted/moles of catalyst. Formula weight of OMS-2 ($\text{KMn}_8\text{O}_{16} \cdot n\text{H}_2\text{O}$) is $734.6 \text{ g} \cdot \text{mol}^{-1}$ (excluding the water).⁶⁰

results showed that the advantages of the present work included low catalyst dosage, no stoichiometric additives and oxidants, and especially the high selectivity towards the target product.

With the optimized conditions in hand, we turned our attention to explore the scope and generality of this selectivity-tunable oxidative dehydrogenation of tetrahydro- β -carbolines over [PW]-OMS-2. Firstly, substrates **1a–1k** were employed with

Table 6 Scope of oxidative dehydrogenation to obtain 1-aryl- β -carbolines^a

Entry	Substrate	Product	Con. (%)	Sel. (%)	TON ^b
1			~100	>99	7.2
2			>99	96	7.2
3			>99	98	7.2
4			>99	>99	7.2
5			>99	84	7.2
6			92	69	6.8
7			95	98	7.0
8			>99	>99	7.2
9			87	88	6.4
10			93	99	6.8
11			84	94	6.2

^a Reaction conditions: substrate (0.2 mmol), [PW]-OMS-2 (20 mg), 1,2-dichlorobenzene (1 mL), air (1 atm), 130 °C, 8 h. ^b Turn over number, TON = moles of tetrahydro- β -carbolines converted/moles of catalyst. The formula weight of OMS-2 ($\text{KMn}_8\text{O}_{16} \cdot n\text{H}_2\text{O}$) is 734.6 g mol^{-1} (excluding the water).⁶⁰

a mixed solvent of acetonitrile/toluene under the optimized conditions for the synthesis of 3,4-dihydro- β -carbolines. As depicted in Table 5, there was no obvious electronic effect of the substituted groups found and a series of substrates were tolerated in the partial oxidative dehydrogenation reaction system. The corresponding 3,4-dihydro- β -carbolines **2a–2k** were successfully formed with good conversion (78–99%) and selectivity (79–99%). Tetrahydro- β -carbolines substituted with heterocycles made the reaction proceed smoothly, although **1k** gave a relatively low conversion (Table 5, **1k**). Next, we ran the dehydrogenation reaction with substrates **1a–1k** in *o*-dichlorobenzene with high temperature over [PW]-OMS-2 for selective obtainment of β -carbolines (Table 6). As expected, β -carbolines with a wide range of substituents were provided smoothly with very high selectivity ranging from 88% to 99%. Unfortunately, **1f** just gave a medium selectivity for β -carboline **2f** (Table 6, **1f**). Remarkably, halogen, methyl, methoxy, naphthyl, pyridyl, quinolyl, and thienyl groups of these desired β -carboline products would be useful handles for further modification to gain other pharmacologically active molecules.

The stability and recyclability of [PW]-OMS-2

The recyclability of the catalyst was also studied *via* the catalytic synthesis of β -carbolines. To ensure the reliability of the catalyst stability test, we correspondingly reduced the amount of catalyst and controlled the reaction at a low conversion (other conditions were maintained under standard reaction conditions). 1-Phenyl-tetrahydro- β -carboline **1a** (0.2 mmol, 50 mg) and [PW]-OMS-2 (3.2 mol%, 5 mg) were placed in a reaction tube, and 1,2-dichlorobenzene (1 mL) was added. Then, the reaction mixture was stirred at 130 °C for 8 h under air. After the reaction, the reaction mixture was cooled and separated by filtration. The used catalyst was collected by filtration and washed with ethyl acetate and ethanol. Then, the retrieved catalyst was placed in an oven and dried at 100 °C for 8 h for the next use. To ensure that the amount of catalyst was sufficient for the next cycle, we carried out parallel reactions. The filtrate was concentrated with a rotary evaporator and the product was purified and obtained by silica gel chromatography. The recycling test showed that [PW]-OMS-2 could be reused at least 5 consecutive times with excellent selectivity (97%–99%) and stable conversion (Fig. 7). Subsequently, the

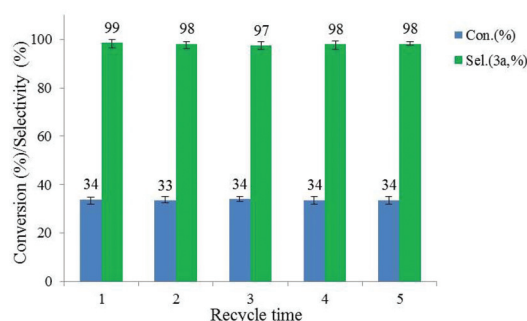
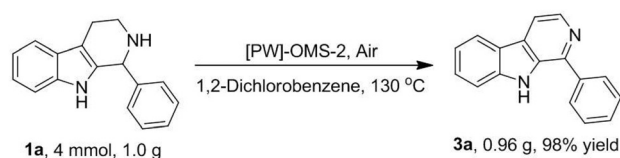


Fig. 7 The recycling experiment.



Scheme 1 Gram-scale reaction.

changes of the retrieved catalyst were measured by XRD, which confirms that the mixed phases of cryptomelane/phosphotungstic acid and crystallinity were retained after five recycles (see ESI Fig. S3†). Importantly, we attempted to realize the synthesis of β -carbolines on a gram-scale reaction with [PW]-OMS-2 and obtained 98% yield of the desired product, which indicates that the heterogeneous catalytic oxidation system is a potential option for practical application (Scheme 1).

Discussion of the mechanism

Based on our experimental results and previous works,⁴⁸ we proposed the possible reaction mechanism that follows the Mars–van Krevelen mechanism (Fig. 8).⁶¹ Firstly, the substrate tetrahydro- β -carboline adsorbed on the catalyst metal Mn^{n+} center and the electron of nitrogen in saturated cycloalkane to active site Mn^{n+} . Then, the formed amine radical species could be subjected to C–H dehydrogenation. The two H atoms on N–H and C–H groups combined with one O atom on the surface of the catalyst to form an H_2O molecule. At the same time, the active site Mn^{n+} was reduced to $Mn^{(n-1)+}$. After desorption of the partial dehydrogenation product 1-aryl-3,4-dihydro- β -carboline and H_2O , the original surface adsorption oxygen formed a surface oxygen vacancy. During the process, O_2 in the atmosphere was necessary to reoxidize the reduced catalyst, replenish the oxygen vacancies and restore the catalytic activity. Thereafter, the imine of the partial dehydrogenation product was transformed to tautomeric cyclic imine and through secondary dehydrogenation the final dehydrogenation product 1-aryl- β -carboline was obtained. The latter catalytic oxidation process is the same as the first step.

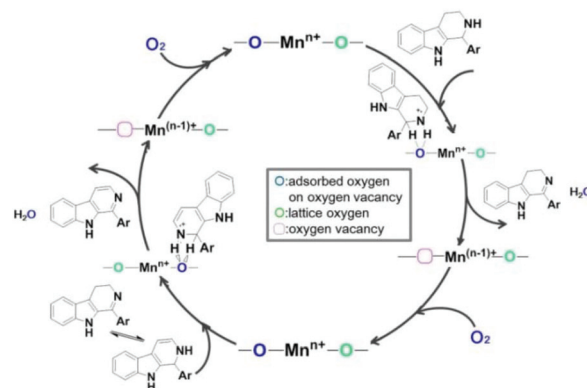


Fig. 8 The proposed reaction mechanism.

The proposed reaction mechanism was verified by experiments. The conversion of the substrate under the nitrogen atmosphere decreased remarkably (35%, Table 3, entry 15) after 8 h, which may be due to a lack of oxygen for re-oxidation of the reduced Mn species. During this process, the labile lattice oxygen was consumed. Additionally, the XPS characterization of [PW]-OMS-2 revealed the amount of lattice oxygen that decreased after reaction under N₂ (Fig. S5, ESI†). On the other hand, under the standard conditions (Table 3, entry 12), the intermediate 1-phenyl-3,4-dihydro-β-carbolines almost completely converted to the complete oxidation product 1-phenyl-β-carbolines within 3 hours. These results are consistent with the abovementioned mechanism.

Conclusions

In conclusion, we have investigated the effects of Mn²⁺ precursors on the preparation of the H₃PO₄·12WO₃/OMS-2 nanocomposite catalyst ([PW]-OMS-2). The catalyst prepared with MnSO₄·H₂O as the Mn²⁺ precursor exhibited a mixed crystal phase, increased surface area (from 67 m² g⁻¹ to 204 m² g⁻¹), abundant surface oxygen vacancy (80.2%) and active lattice oxygen species which led to excellent catalytic performance. Through the optimization of reaction conditions, we first successfully developed selectivity-tunable reaction systems to obtain pharmaceutically active compounds 3,4-dihydro-β-carbolines and β-carbolines with excellent selectivity (up to 99%) employing air as an effective oxidant. The synthetic strategy possessed the advantages of the use of non-noble metals and recyclable catalysts, being selectivity-tunable and having broad substrate scope, and it could be used as an alternative to the traditional synthesis methods. More importantly, under a highly active catalyst, the research and optimization of solvents might be an efficient pathway to improve the selectivity of the catalytic oxidative reaction.

Conflicts of interest

There are no conflicts to declare.

Acknowledgements

We gratefully acknowledge the National Natural Science Foundation of China (Grant No. 21403256 and 21573261), the Youth Innovation Promotion Association CAS (2018456) and LICP Cooperation Foundation for Young Scholars (HZJJ20-10).

Notes and references

- W. D. Inman, W. M. Bray, N. C. Gassner, R. S. Lokey, K. Tenney, Y. Y. Shen, K. Tendyke, T. Suh and P. Crews, *J. Nat. Prod.*, 2010, **73**, 255–257.
- K. Patel, M. Gadewar, R. Tripathi, S. K. Prasad and D. K. Patel, *Asian Pac. J. Trop. Biomed.*, 2012, **2**, 660–664.
- X. Yu, W. Lin, J. Li and M. Yang, *Bioorg. Med. Chem. Lett.*, 2004, **14**, 3127–3130.
- R. B. Volk and F. H. Furkert, *Microbiol. Res.*, 2006, **161**, 180–186.
- A. Kamal, V. Srinivasulu, V. L. Nayak, M. Sathish, N. Shankaraiah, C. Bagul, N. V. Reddy, N. Rangaraj and N. Nagesh, *ChemMedChem*, 2014, **9**, 2084–2098.
- L. Gupta, K. Srivastava, S. Singh, S. K. Puri and P. M. Chauhan, *Bioorg. Med. Chem. Lett.*, 2008, **18**, 3306–3309.
- W. Horton, A. Sood, S. Peerannawar, N. Kugyela, A. Kulkarni, R. Tulsan, C. D. Tran, J. Soule, H. LeVine 3rd, B. Torok and M. Torok, *Bioorg. Med. Chem. Lett.*, 2017, **27**, 232–236.
- R. Otto, R. Penzis, F. Gaube, T. Winckler, D. Appenroth, C. Fleck, C. Trankle, J. Lehmann and C. Enzensperger, *Eur. J. Med. Chem.*, 2014, **87**, 63–70.
- J. Stockigt, A. P. Antonchick, F. Wu and H. Waldmann, *Angew. Chem., Int. Ed.*, 2011, **50**, 8538–8564.
- K. L. Manasa, Y. Tangella, G. Ramu and B. Nagendra Babu, *ChemistrySelect*, 2017, **2**, 9162–9167.
- P. Ábrányi-Balogh, T. Földesi, A. Grün, B. Volk, G. Keglevich and M. Milen, *Tetrahedron Lett.*, 2016, **57**, 1953–1957.
- P. Ashok, S. Chander, A. Tejeria, L. Garcia-Calvo, R. Balana-Fouce and S. Murugesan, *Eur. J. Med. Chem.*, 2016, **123**, 814–821.
- S. D. Durham, B. Sierra, M. J. Gomez, J. K. Tran, M. O. Anderson, N. A. Whittington-Davis and S. Eagon, *Tetrahedron Lett.*, 2017, **58**, 2747–2750.
- Q. Chen, C. Ji, Y. Song, H. Huang, J. Ma, X. Tian and J. Ju, *Angew. Chem., Int. Ed.*, 2013, **52**, 9980–9984.
- S. U. Dighe, S. Khan, I. Soni, P. Jain, S. Shukla, R. Yadav, P. Sen, S. M. Meeran and S. Batra, *J. Med. Chem.*, 2015, **58**, 3485–3499.
- S. V. Gaikwad, D. N. Nadimetla, M. A. Kobaisi, M. Devkate, R. Joshi, R. G. Shinde, M. V. Gaikwad, M. D. Nikalje, S. V. Bhosale and P. D. Lokhande, *ChemistrySelect*, 2019, **4**, 10054–10059.
- S. Hati and S. Sen, *Tetrahedron Lett.*, 2016, **57**, 1040–1043.
- R. S. Kusrkar and S. K. Goswami, *Tetrahedron*, 2004, **60**, 5315–5318.
- G. Lin, Y. Wang, Q. Zhou, W. Tang, J. Wang and T. Lu, *Molecules*, 2010, **15**, 5680–5691.
- Y. Ling, C. Xu, L. Luo, J. Cao, J. Feng, Y. Xue, Q. Zhu, C. Ju, F. Li, Y. Zhang, Y. Zhang and X. Ling, *J. Med. Chem.*, 2015, **58**, 9214–9227.
- A. Kamal, Y. Tangella, K. L. Manasa, M. Sathish, V. Srinivasulu, J. Chetna and A. Alarifi, *Org. Biomol. Chem.*, 2015, **13**, 8652–8662.
- S. Wang and M. Wu, *Synthesis*, 2009, 587–592.
- S. Gaikwad, D. Kamble and P. Lokhande, *Tetrahedron Lett.*, 2018, **59**, 2387–2392.
- Y. Schott, M. Decker, H. Rommelspacher and J. Lehmann, *Bioorg. Med. Chem. Lett.*, 2006, **16**, 5840–5843.

- 25 B. Xin, W. Tang, Y. Wang, G. Lin, H. Liu, Y. Jiao, Y. Zhu, H. Yuan, Y. Chen and T. Lu, *Bioorg. Med. Chem. Lett.*, 2012, **22**, 4783–4786.
- 26 W. Yin, S. Majumder, T. Clayton, S. Petrou, M. L. VanLinn, O. A. Namjoshi, C. Ma, B. A. Cromer, B. L. Roth, D. M. Platt and J. M. Cook, *Bioorg. Med. Chem.*, 2010, **18**, 7548–7564.
- 27 B. Bai, X. Y. Li, L. Liu, Y. Li and H. J. Zhu, *Bioorg. Med. Chem. Lett.*, 2014, **24**, 96–98.
- 28 R. Ikeda, T. Kimura, T. Tsutsumi, S. Tamura, N. Sakai and T. Konakahara, *Bioorg. Med. Chem. Lett.*, 2012, **22**, 3506–3515.
- 29 G. K. Prakash, T. Mathew, D. Hoole, P. M. Esteves, Q. Wang, G. Rasul and G. A. Olah, *J. Am. Chem. Soc.*, 2004, **126**, 15770–15776.
- 30 C. Y. Chen, T. Andreani and H. Li, *Org. Lett.*, 2011, **13**, 6300–6303.
- 31 J. D. Panarese and S. P. Waters, *Org. Lett.*, 2010, **12**, 4086–4089.
- 32 L. R. Pahalagedara, S. Dharmarathna, C. K. King'onde, M. N. Pahalagedara, Y. T. Meng, C. H. Kuo and S. L. Suib, *J. Phys. Chem. C*, 2014, **118**, 20363–20373.
- 33 E. K. Nyutu, C.-H. Chen, S. Sithambaram, V. M. B. Crisostomo and S. L. Suib, *J. Phys. Chem. C*, 2008, **112**, 6786–6793.
- 34 H. Huang, Y. Meng, A. Labonte, A. Doble and S. L. Suib, *J. Phys. Chem. C*, 2013, **117**, 25352–25359.
- 35 A. Iyer, J. Del-Pilar, C. K. King'onde, E. Kissel, H. F. Garces, H. Huang, A. M. El-Sawy, P. K. Dutta and S. L. Suib, *J. Phys. Chem. C*, 2012, **116**, 6474–6483.
- 36 J. Hou, L. Liu, Y. Li, M. Mao, H. Lv and X. Zhao, *Environ. Sci. Technol.*, 2013, **47**, 13730–13736.
- 37 H. C. Genuino, S. Dharmarathna, E. C. Njagi, M. C. Mei and S. L. Suib, *J. Phys. Chem. C*, 2012, **116**, 12066–12078.
- 38 B. Hu, C.-H. Chen, S. J. Frueh, L. Jin, R. Joesten and S. L. Suib, *J. Phys. Chem. C*, 2010, **114**, 9835–9844.
- 39 N. N. Opembe, C. K. King'onde, A. E. Espinal, C.-H. Chen, E. K. Nyutu, V. M. Crisostomo and S. L. Suib, *J. Phys. Chem. C*, 2010, **114**, 14417–14426.
- 40 S. L. Suib, *Acc. Chem. Res.*, 2008, **41**, 479–487.
- 41 G. Elmaci, C. E. Frey, P. Kurz and B. Zümreoglu-Karan, *J. Mater. Chem. A*, 2016, **4**, 8812–8821.
- 42 G. Elmaci, O. Icten, A. N. Ay and B. Zümreoglu-Karan, *Appl. Clay Sci.*, 2015, **107**, 117–121.
- 43 G. Elmaci, A. S. Ertürk, M. Sevim and Ö. Metin, *Int. J. Hydrogen Energy*, 2019, **44**, 17995–18006.
- 44 G. Elmaci, S. Cerci and D. Sunar-Cerci, *J. Mol. Struct.*, 2019, **1195**, 632–640.
- 45 X. Li, J. Ma, X. Jia, F. Xia, Y. Huang, Y. Xu and J. Xu, *ACS Sustainable Chem. Eng.*, 2018, **6**, 8048–8054.
- 46 X. Jia, J. Ma, F. Xia, M. Gao, J. Gao and J. Xu, *Nat. Commun.*, 2019, **10**, 2338.
- 47 X. Meng, J. Zhang, B. Chen, Z. Jing and P. Zhao, *Catal. Sci. Technol.*, 2016, **6**, 890–896.
- 48 X. Bi, T. Tang, X. Meng, M. Gou, X. Liu and P. Zhao, *Catal. Sci. Technol.*, 2020, **10**, 360–371.
- 49 X. Meng, C. Yu, G. Chen and P. Zhao, *Catal. Sci. Technol.*, 2015, **5**, 372–379.
- 50 X. Meng, Y. Wang, Y. Wang, B. Chen, Z. Jing, G. Chen and P. Zhao, *J. Org. Chem.*, 2017, **82**, 6922–6931.
- 51 X. Meng, X. Bi, C. Yu, G. Chen, B. Chen, Z. Jing and P. Zhao, *Green Chem.*, 2018, **20**, 4638–4644.
- 52 C. Wang, J. Ma, F. Liu, H. He and R. Zhang, *J. Phys. Chem. C*, 2015, **119**, 23119–23126.
- 53 X. F. Shen, Y. S. Ding, J. Liu, Z. H. Han, J. I. Budnick, W. A. Hines and S. L. Suib, *J. Am. Chem. Soc.*, 2005, **127**, 6166–6167.
- 54 G. Yan, Y. Lian, Y. Gu, C. Yang, H. Sun, Q. Mu, Q. Li, W. Zhu, X. Zheng, M. Chen, J. Zhu, Z. Deng and Y. Peng, *ACS Catal.*, 2018, **8**, 10137–10147.
- 55 Y. Xu, J. Dhainaut, G. Rochard, J.-P. Dacquin, A.-S. Mamede, J.-M. Giraudon, J.-F. Lamonier, H. Zhang and S. Royer, *Chem. Eng. J.*, 2020, **388**, 124146.
- 56 W. Hong, M. Shao, T. Zhu, H. Wang, Y. Sun, F. Shen and X. Li, *Appl. Catal., B*, 2020, **274**, 119088.
- 57 Z. X. Wang, J. C. Xiang, Y. Cheng, J. T. Ma, Y. D. Wu and A. X. Wu, *J. Org. Chem.*, 2018, **83**, 12247–12254.
- 58 B. Zheng, T. H. Trieu, T.-Z. Meng, X. Lu, J. Dong, Q. Zhang and X.-X. Shi, *RSC Adv.*, 2018, **8**, 6834–6839.
- 59 A. Kamal, M. Sathish, A. V. G. Prasanthi, J. Chetna, Y. Tangella, V. Srinivasulu, N. Shankaraiah and A. Alarifi, *RSC Adv.*, 2015, **5**, 90121–90126.
- 60 M. Kakazey, N. Ivanova, Y. Boldurev, S. Ivanov, G. Sokolsky, J. G. Gonzalez-Rodriguez and M. Vlasova, *J. Power Sources*, 2003, **114**, 170–175.
- 61 K. Mullick, S. Biswas, A. M. Angeles-Boza and S. L. Suib, *Chem. Commun.*, 2017, **53**, 2256–2259.